Journal of Solid State Chemistry **153,** 282–286 (2000)
doi:10.1006/jssc.2000.8759, available online at http://www.idealibrary.com on IDEAL®

NMR Study of Ionic Distribution in Li-Doped BPO_4

A. J. Dodd and E. R. H. van Eck[1]

Centre for Materials Research, School of Physical Sciences, University of Kent, Canterbury, Kent CT2 7NR, United Kingdom

and

M. J. G. Jak, E. M. Kelder, and J. Schoonman

Delft Interfaculty Research Centre, Renewable Energy, Laboratory for Inorganic Chemistry, Delft University of Technology, Julianalaan 136, 2628 BL Delft, The Netherlands

Received February 15, 2000; in revised form April 20, 2000; accepted May 4, 2000; published online July 17, 2000

^{7}Li nuclear magnetic resonance studies of a series of lithium-doped boron phosphates ($Li_xB_{1-x/3}PO_4$, $0<x<0.2$) are reported. Second moment calculations have been made using basic structural models and have been used in conjunction with experimental data to present a model for the distribution of Li ions in the lattice. It is shown that Li ions form in clusters, most likely around a boron vacancy. High-temperature measurements are used to obtain ionic mobility as a function of concentration, and activation energy for hopping of Li ions is shown to increase with concentration. © 2000 Academic Press

Key Words: **NMR; Li-doped BPO_4; second moment; clustering; ceramic electrolyte.**

INTRODUCTION

Detailed studies of the structure of undoped BPO_4 have been carried out since the late 1930s and its properties are well known. More recent work by Kelder *et al.* (1) has shown that Li-doped BPO_4 has applications as a ceramic electrolyte for Li-ion rechargeable batteries. Current Li-ion batteries outclass conventional systems in areas such as energy density and cell voltage; however, most systems use liquid- or polymer-based electrolytes, which are unstable at temperatures exceeding 50°C, posing safety problems as well as poor performance. The nanocrystalline ceramic electrolyte studied here is a less expensive and safer material for use at high temperatures and is expected to be used up to temperatures around 200°C.

The structure of Li-doped BPO_4 has been extensively studied (2–4) and two possible defect models have been derived, shown here using the Kröger–Vink notation:

$$V_B''' + 3Li_i,$$

$$Li_B'' + 2Li_i.$$

However, a model for the distribution of ions within the lattice has not been reported before. Using ^{7}Li NMR relaxation and linewidth measurements on a series of samples with doping levels up to $x = 0.2$ (referred to as 20 mol% hereafter), such a model is derived.

Solid-state batteries using the ceramic electrolyte studied here are intended for use at temperatures around 473 K. NMR spectra were also obtained over a range of temperatures up to 453 K to study the mobility of Li ions near the expected operating temperature. This is of particular interest for the bulk mobility of these materials since in the high-temperature region in which they are designed to be used bulk conductivity is thought to be the main conduction mechanism (5). NMR is a commonly used tool in the study of bulk mobility, which is directly related to conductivity by the Nernst–Einstein equation (5).

Work by Jak *et al.* (2–4) has shown that three-dimensional channels exist within the high-cristobalite structure of BPO_4, as can be seen in Fig. 1. It is through these channels that bulk conductivity takes place, and it is within the channels that the interstitial Li ions are found (2).

EXPERIMENTAL

Sample Preparation

A series of $Li_xB_{1-x/3}PO_4$ samples with doping levels of 2, 5, 7, 10, 15, and 20 mol% were prepared using the P_2O_5 synthesis route described in (6). Undoped BPO_4 is a patented desiccant due to its strong hygroscopic nature. Proton

[1]To whom correspondence should be addressed. E-mail: erhv@ukc.ac.uk. Fax: +44 (0) 1227 827 558.

0022-4596/00 $35.00

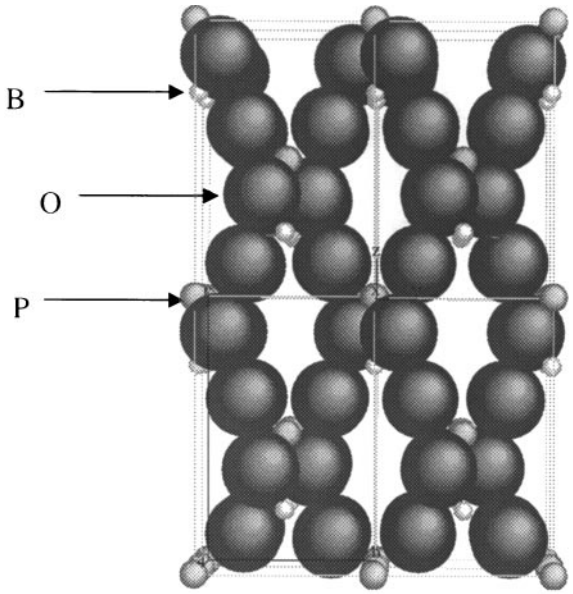

FIG. 1. Crystal structure of undoped BPO_4 showing conduction channels (oxygen ions not to scale for clear indication of channel position).

coupling was seen to strongly affect the ^{7}Li linewidth at the rigid lattice temperature, and the presence of water also had an effect on the Li ion mobility at higher temperatures. All samples were dried at 150°C in a furnace for 24 h and then transferred to a vacuum oven at 30 mm Hg and 150°C for an additional 3 h. The powder was then immediately placed into the sample tube and sealed with Teflon tape to ensure that no water was present. Proton NMR before and after drying showed that the water content in the dried samples was negligible. Repeated drying and subsequent linewidth measurements verified the reproducibility of the results. It can therefore be safely assumed that the ^{7}Li linewidth measurements are not affected by dipolar coupling to protons.

XRD spectra show that Li-doped BPO_4 exists as a single-phase material up to a doping of 20 mol% Li. At 30 mol% (not used in this study) a small fraction of second-phase material is found (5).

^{7}Li NMR

The ^{7}Li NMR data were obtained using a Chemagnetics CMX300 spectrometer with the 7.05-T magnet giving a ^{7}Li resonance frequency of 116.68 MHz. A single-pulse sequence was used with a 90° pulse of 2 μs (r–f field strength of 125 kHz). All spectra were acquired without spinning using a 4-mm HX double-resonance MAS probe. Temperature was controlled using the Chemagnetics temperature controller, which is thought to be accurate to ± 0.1 K. Samples were left for a minimum of 5 min to reach the target temperature, which is ample time for equilibrium to be reached. Rigid lattice measurements were made at a temperature of 123 K and additional measurements were made at 223, 248, 273, 298, and 313 and increasing in increments of 20 to 453 K. Full width at half maximum (FWHM) values were ascertained using MATLAB (7), and lineshapes were checked using the spectrometer software. Intermolecular distances used in second-moment calculations were found using the Ca.R.Ine Crystallography software (8).

THEORETICAL CONSIDERATIONS

^{7}Li Characteristics

Diffusion of the mobile lithium ions within the lattice has a pronounced effect on both the shape and the width of the ^{7}Li NMR spectra. At rigid lattice temperatures the lineshape is entirely Gaussian, whereas at higher temperatures when motional narrowing is introduced the shape tends toward the Lorentzian. Lithium is a quadrupolar nucleus ($I = 3/2$). In general, the NMR lineshape of a quadrupolar nucleus is determined by dipolar and quadrupolar interactions and chemical shift anisotropy (CSA). However the ^{7}Li nucleus has a very small chemical shift range (9) and a small quadrupole moment (-4.1×10^{-30} m^2) (10). Thus, the predominant broadening mechanism for the ^{7}Li nucleus is through homo- and heteronuclear dipolar coupling. Both CSA and quadrupolar coupling can be ignored (11). The ^{7}Li atoms in the crystal are found at interstitial sites within the conduction channels or at a boron vacancy (2); in either of these positions dipolar coupling with ^{31}P and ^{11}B is strong, and the coupling with other ^{7}Li nuclei whose positions are not known is to be considered by calculation and experiment. Since the natural abundance of ^{17}O is only 0.037%, this coupling will be negligible and is ignored; however, the coupling with the 19.58% abundant ^{10}B is taken into account.

Second Moments

The magnitude of dipolar coupling is usually expressed in terms of the second moment, M_2, which represents the mean square local field at the nucleus due to dipolar interactions. The second moment can also be represented in frequency terms and the required form for the Van Vleck equations (12) due to the coupling between like and unlike nuclei can be written as

$$M_2 = M_2^{\text{II}} + M_2^{\text{IS}}, \qquad [1]$$

where

$$M_2^{\text{II}} = \frac{3}{5} I(I+1)\gamma_I^4 \hbar^2 \left(\frac{\mu_0}{4\pi}\right)^2 \sum \frac{(1-3\cos^2\theta)^2}{r^6}. \qquad [2a]$$

Here, M_2^{II} represents the coupling due to homonuclear interactions between like spins, with modifications made for the spin 3/2 ^{7}Li nuclei in inequivalent sites (11), and

$$M_2^{\mathrm{IS}} = \frac{1}{3} S(S+1)\gamma_I^2\gamma_S^2\hbar^2 \left(\frac{\mu_0}{4\pi}\right)^2 \sum \frac{(1-3\cos^2\theta)^2}{r^6}, \quad [2b]$$

where M_2^{IS} gives the heteronuclear contribution between unlike spins. In Eqs. [2a] and [2b] γ represents the gyromagnetic ratio of the nucleus and r is the internuclear distance. For a powder sample the following approximation can made (13):

$$\langle (1-3\cos^2\theta)^2 \rangle = \frac{4}{5}.$$

Furthermore, for the Gaussian frequency distribution found here the second moment can be directly related to linewidth (13) since

$$M_2 = \sigma^2,$$

where σ^2 is the mean square width of the distribution from which the FWHM value of the peak is easily found since (14)

$$\mathrm{FWHM} = 2.36\sigma.$$

In this way second moments can be derived from linewidth measurements.

With its inverse relationship to the sixth power of nuclear distance the second moment is a powerful tool for use in considering the distribution of ions introduced into a material after doping. Second moments can only be considered at rigid lattice temperatures, when no ionic motion is taking place.

The Motional Narrowing Regime

At temperatures above 300 K the resonance line of the ^{7}Li nucleus narrows rapidly due to the reduction in interactions with the local magnetic fields, which results from motion. The linewidth ($\Delta\omega$) after the onset of motional narrowing is directly related to atomic jump time τ (15), and of course if the jump time is shorter, the mobility is higher,

$$\Delta\omega = (\Delta\omega_{\mathrm{rl}})^2\tau, \quad [3]$$

where $\Delta\omega_{\mathrm{rl}}$ is the rigid lattice linewidth. Furthermore, in the linear section of the graph of ln $\Delta\omega$ versus inverse temperature after the onset of motional narrowing the gradient is used in the calculation of activation energy since

$$\Delta\omega = \Delta\omega_0 e^{E_a/kT}, \quad [4]$$

where E_a is the activation energy for hopping of ^{7}Li ions between sites and $\Delta\omega_0$ is the linewidth at infinite temperature.

RESULTS AND DISCUSSION

Figure 2 shows a typical ^{7}Li spectrum obtained in the rigid lattice limit for the 10 mol% sample. It is overlaid with a Gaussian fitting function as an example of the Gaussian lineshape obtained for ^{7}Li at rigid lattice temperatures.

Second-moment calculations for heteronuclear coupling were made for Li ions at both the interstitial and vacancy site. Values were then scaled under the assumption that each boron vacancy was charge balanced by a Li^+ ion at the vacancy and by two interstitial Li ions situated in the conduction channels. The interstitial site with coordinates (0.5, 0.0, 0.2) was found by Rietveld refinement of XRD data for the 20 mol% sample (2). Coupling with the 20% abundant ^{10}B nucleus was taken into account, as was the depletion of boron with increasing Li concentration, although this proved to be negligible. Calculations were made for coupling with all unlike nuclei within a 10-Å sphere. Since the second moment is inversely proportional to the sixth power of distance, any interactions further away than 10 Å will be negligible. The total heteronuclear component of the second moment M_2^{IS} was found to be 0.71×10^8 rad^2 s^{-2} using Eq. [2b]. This would correspond to a frequency

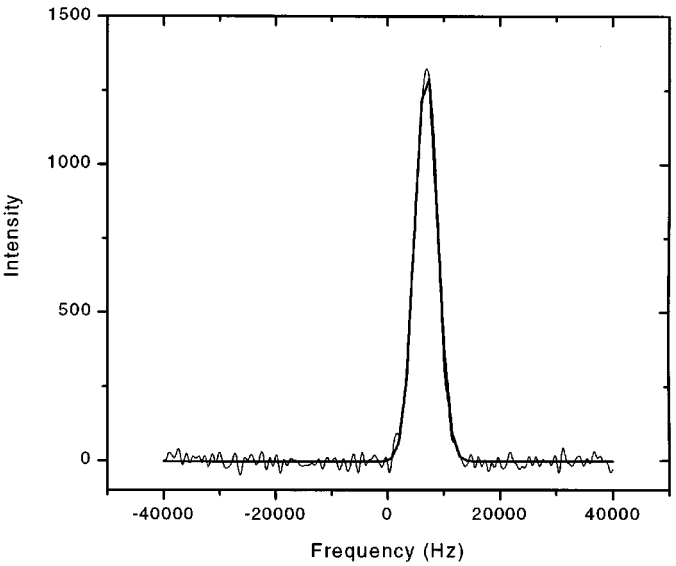

FIG. 2. Gaussian lineshape of ^{7}Li spectrum for 10 mol% sample at 123 K.

broadening of the ^{7}Li line of 3.17 kHz, assuming a Gaussian lineshape.

To consider the total second moment, one also needs to know the second-moment contribution M_2^{II} due to homonuclear interactions. The distribution of Li ions in the BPO_4 structure is not known, and so models for homogeneous and random distribution of ions were made and second moments were calculated for all samples.

In the homogeneous model Li atoms are placed on a cubic lattice for which the spacing is determined from the Li concentration. In the random model a 10-Å sphere was again used and possible sites were randomly filled within this sphere; the number of ions used was altered according to the concentration. For the random model, which is the more physically real of the two models, M_2^{II} varies linearly from zero at 0 mol% to 0.15×10^8 rad^2 s^{-2} at 20 mol% Li. Figure 3 shows the total calculated second moments of both models and the experimental data for all samples at 123 K. Both models and the experimental data for all samples at 123 K. Both models show only a small increase in the second moment over the range of doping used compared with the experimental results obtained.

The difference in magnitude between experimental results and the calculated values can only be due to clustering of Li ions. By extrapolating the results in Fig. 3 to a "0 mol%" doping, it is possible to make a crude estimate of Li–Li distance when only one cluster exists. Such a calculation reveals a distance of (3.0 ± 0.3) Å between interacting Li ions, assuming a cluster size of three ions, which is expected to be an underestimate since intercluster broadening is not considered. The shortest possible distance between a vacancy site and an interstitial ion is 3.08 Å. The most natural model for such a cluster would be for one Li to be at a vacancy site with two interstitial Li ions in neighboring conduction channels, charge balancing the boron vacancy.

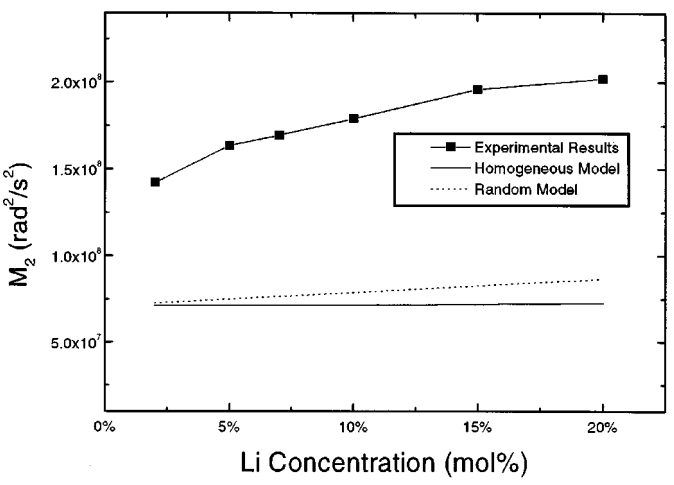

FIG. 3. Second-moment values ($M_2 = M_2^{II} + M_2^{IS}$) as a function of molar Li concentration, calculated using a random site filling model and homogeneous distribution model. Experimental data at 123 K are also shown.

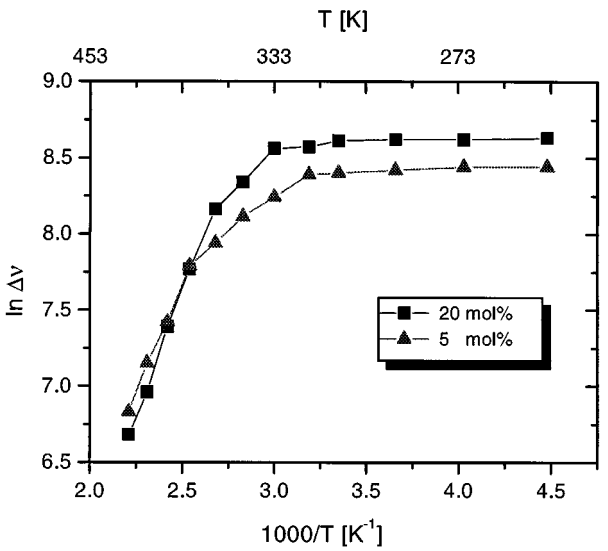

FIG. 4. Temperature dependence of ^{7}Li linewidth for 5 and 20 mol% sample.

The difference in line broadening seen between the 2 and 20 mol% sample can be attributed to the additional intercluster interactions and may also be indicative of a slight contraction in cluster dimensions.

Figure 4 shows the motional narrowing of the 5 and 20 mol% samples, illustrating the difference in rigid lattice linewidth and the extent of motional narrowing observed. Using Eq. [3], atomic jump times are calculated in the high-temperature region, and Fig. 5 demonstrates the variation of jump time as a function of concentration at 453 K. These data show a minimum jump time of 4.7 μs at a doping of 10 mol%, indicating a maximum in mobility; the variation trend is the same at all temperature points in the motionally

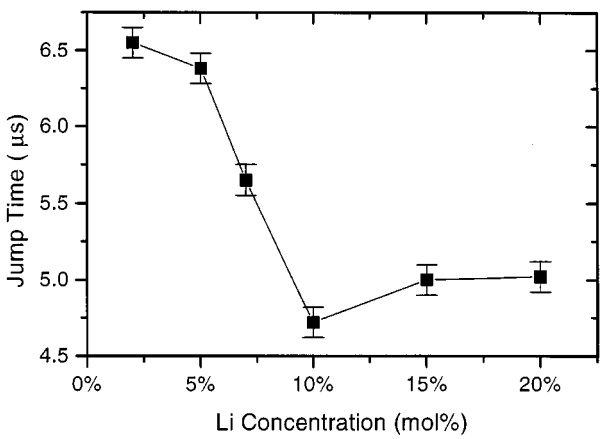

FIG. 5. Atomic jump time (τ) as a function of molar Li concentration at 453 K.

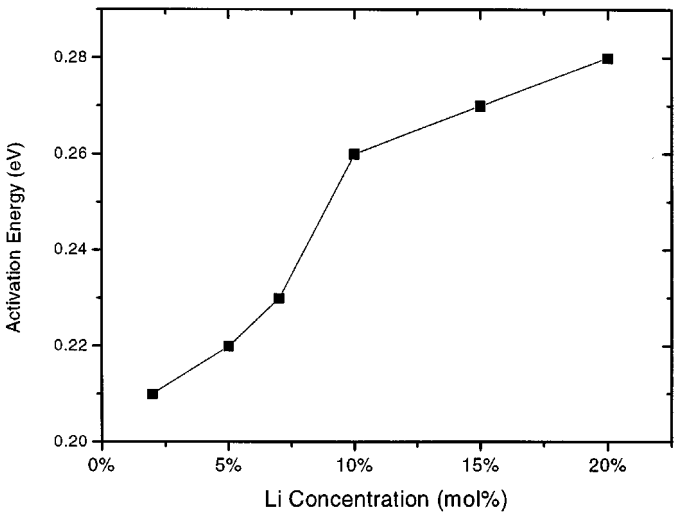

FIG. 6. Activation energy for hopping of Li^+ ions as a function of Li doping level.

narrowed region. The maximum in mobility at 10 mol% coincides with a maximum in aperture of the proposed conduction channels (5).

From the high-temperature data the activation energy for atomic jumps was calculated. Figure 6 shows an increase in activation energy with increasing Li concentration. This increasing trend is most likely due to increasing electrostatic repulsion as neighboring clusters are brought closer together. At 20 mol% the activation energy is found to be 0.28 eV, in good agreement with AC-IS data, which find an activation energy of 0.3 eV (5).

CONCLUSIONS

The rigid lattice ^{7}Li NMR data for the second moment compared with the calculated values from both the random and homogeneous distribution models show that Li clusters exist with an internuclear distance of around 3 Å. Furthermore, M_2 is seen to increase across the range of samples to 20 mol% Li, which is due to the interactions between clusters and a possible contraction in cluster dimensions due to electrostatic repulsion. The most natural configuration of Li ions within such a cluster is one where a Li ion is fixed at the boron vacancy and an additional two ions are found in the conduction channels surrounding the vacancy site, though it is not yet possible to report with certainty the number of interstitials in the cluster. Clearly, further research is needed in this area.

From atomic jump time data it is found that ionic mobility of Li is a maximum at 10 mol% doping, indicating that the bulk conductivity in the 10 mol% sample is highest at high temperatures. The activation energy is found to increase with concentration, probably due to electrostatic repulsion.

ACKNOWLEDGMENTS

Financial support from the Engineering and Physical Sciences Research Council (EPSRC) and travel support from the European Science Foundation (ESF) are gratefully acknowledged. The ESF-NANO programme is also acknowledged. Thanks also go to J. H. Strange for valuable discussions.

REFERENCES

1. E. M. Kelder, M. J. G. Jak, F. de Lange, and J. Schoonman, *Solid State Ionics* **85,** 285 (1996).
2. M. J. G. Jak, E. M. Kelder, Z. A. Kaskur, J. Pielaszek, and J. Schoonman, *Solid State Ionics* **119,** 159 (1998).
3. M. J. G. Jak, E. M. Kelder, and J. Schoonman, *J. Solid State Chem.* **142,** 74–79 (1999).
4. M. J. G. Jak, V. W. J. Verhoeven, I. M. de Schepper, F. M. Mulder, E. M. Kelder, and J. Schoonman, *Physica B* **266,** 108 (1999).
5. M. J. G. Jak, "Dynamic Compaction of Li-Ion Battery Components and Batteries." Ph.D. thesis, Delft University of Technology, Universal Press, Veenendaal, 1999.
6. M. J. G. Jak, E. M. Kelder, J. Schoonman, N. M. Van der Pers, and A. Weisenburger, *J. Electroceram.* **2**(2), 127–134 (1998).
7. "MATLAB version 5.02." MathWorks Inc, 1998.
8. "Ca.R.Ine Crystallography version 3.1." 1998.
9. C. Brevard and P. Granger, "Handbook of High Resolution Multinuclear NMR." Wiley, New York, 1981.
10. A. T-W. Yap and S. R. Elliott, *J. Non Cryst. Solids* **192/193,** 207–211 (1995).
11. E. Göbel, W. Müller Warmuth, H. Olyschläger, and H. Dutz, *J. Magn. Reson.* **36,** 371–387 (1979).
12. J. H. Van Vleck, *Phys. Rev.* **74,** 1168–1183 (1948).
13. R. K. Harris, "NMR Spectroscopy." Wiley, New York, 1987.
14. E. Fukushima, "Experimental Pulse NMR." Addison–Wesley, Reading, MA, 1981.
15. C. P. Slichter, "Principles of Magnetic Resonance." Springer-Verlag, New York, 1992.